Geochimica et Cosmochimica Acta, Vol. 69, No. 13, pp. 3237–3248, 2005

0016-7037/05 $30.00 + .00

doi:10.1016/j.gca.2005.01.030

Experimental and theoretical vibrational spectroscopy studies of acetohydroxamic acid and desferrioxamine B in aqueous solution: Effects of pH and iron complexation

David C. Edwards,[1,*] Steen B. Nielsen,[1] Andrzej A. Jarzęcki,[1,†] Thomas G. Spiro,[1] and Satish C. B. Myneni[2,3]

[1]Department of Chemistry, Princeton University, Frick Laboratory, Princeton, NJ 08544, USA
[2]Department of Geosciences, Princeton University, Guyot Hall, Princeton, NJ 08544, USA
[3]Earth Sciences Division, Lawrence Berkeley National Laboratory, Berkeley, CA 94720, USA

(*Received March* 25, 2004; *accepted in revised form January* 12, 2005)

Abstract—The deprotonation and iron complexation of the hydroxamate siderophore, desferrioxamine B (desB), and a model hydroxamate ligand, acetohydroxamic acid (aHa), were studied using infrared, resonance Raman and UV-vis spectroscopy. The experimental spectra were interpreted by a comparison with DFT calculated spectra of aHa (partly hydrated) and desB (reactive groups of unhydrated molecule) at the B3LYP/6-31G* level of theory. The ab initio models include three water molecules surrounding the deprotonation site of aHa to account for partial hydration. Experiments and calculations were also conducted in D_2O to verify spectral assignments. These studies of aHa suggest that the *cis*-keto-aHa is the dominant form, and its deprotonation occurs at the oxime oxygen atom in aqueous solutions. The stable form of iron-complexed aHa is identified as $Fe(aHa)_3$ for a wide range of pH conditions. The spectral information of aHa and an ab initio model of desB were used to interpret the chemical state of different functional groups in desB. Vibrational spectra of desB indicate that the oxime and amide carbonyl groups can be identified unambiguously. Vibrational spectral analysis of the oxime carbonyl after deprotonation and iron complexation of desB indicates that the conformational changes between anion and the iron-complexed anion are small. Enhanced electron delocalization in the oxime group of Fe-desB when compared to that of $Fe(aHa)_3$ may be responsible for higher stability constant of the former.

1. INTRODUCTION

The chemistry of biomacromolecules influences the dissolution of minerals, solubility and redox cycling of metals, and the acquisition of metals by organisms (Neilands, 1981; Hersman et al., 1995; Holmen et al., 1997; Barbeau et al., 2001). Of the different macromolecules, siderophores are important because of their common occurrence in terrestrial and marine systems, and their high metal complexation characteristics. Bacteria secrete siderophores to obtain iron for metabolic purposes in iron-limiting situations (Neilands, 1981; Bossier et al., 1988; Matzanke et al., 1989). Because of their strong binding ability, siderophores can also affect the ligand-promoted dissolution of iron(III) hydr(oxides) and alter the geochemical cycling of iron in the environment (Stumm and Salzburger, 1992; Hersman et al., 1995; Holmen et al., 1997; Kraemer et al., 1999; Kalinowski et al., 2000). The high stability constants of siderophore-metal complexes also make them amenable for applications in the extraction, concentration and remediation of metal contaminated soils and sediments at waste repositories (Brainard et al., 1992), and in the treatment of siderosis (Bergeron and Brittenham, 1994). Information on the coordination environment and the chemical state of Fe-siderophore complex is central to the evaluation of the role of siderophores in the aforesaid processes. A detailed understanding of the molecular behavior of siderophores in aqueous solutions and at mineral-water interfaces is necessary to assess their role in different biogeochemical processes in the environment. Here we present an experimental and theoretical investigation of the functional group chemistry of a hydroxamate siderophore (desferrioxamine B, desB) and its iron complexation behavior in aqueous solutions.

Characterization of siderophores in conditions representative of natural systems has been difficult due to their low concentration and interference from other organic species. Recently, researchers began isolating siderophores from natural samples and characterizing their crystalline Fe complexes using X-ray crystallography (vanderHelm and Poling, 1976; Hossain et al., 1983; Hossain et al., 1998; Dhungana et al., 2001). In addition, researchers are using smaller molecules, which contain the same functional groups as siderophores, to understand the behavior of siderophores (Santos et al., 1993; Farkas et al., 1999). Several studies have also indicated that infrared spectroscopy is an ideal tool to examine the functional group chemistry of organic molecules and their metal complexes (Holmen et al., 1997; Boily et al., 2000; Loring et al., 2000; Duckworth and Martin, 2001; Strathmann and Myneni, 2004). However, the structure of the metal complex is difficult to assess when the complexed ligand has multiple functional groups with overlapping infrared absorption transitions. To overcome this situation, we used resonance Raman spectroscopy, a technique sensitive to the coordination environment around the metal in a metal-siderophore complex.

Among the different siderophores in the environment, desB is particularly interesting because of its ubiquity (Fig. 1). The concentration of desB varies in natural environments, with concentrations as high as micromolar levels in the soil rhizosphere, and nanomolar concentrations in seawater (Powell et al., 1980; Bergeron and Pegram, 1988). In aqueous solution,

* Author to whom correspondence should be addressed (dcedward@princeton.edu).
† *Present address:* Chemistry Department, the Brooklyn College and the Graduate School of the City University of New York, Brooklyn, NY 11210, USA.

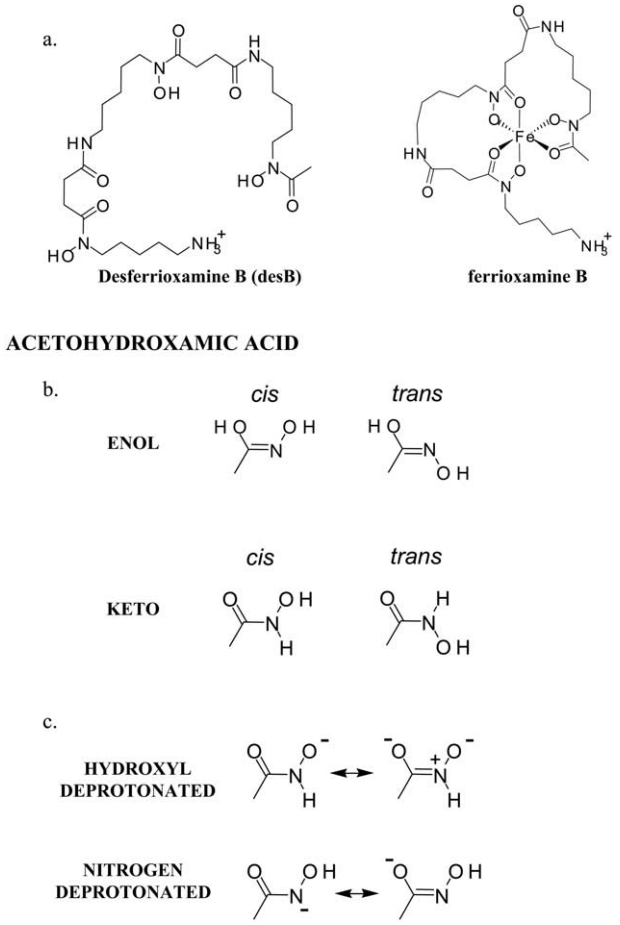

Fig. 1. Graphical representations of different forms of aHa and desB. (a) Desferrioxamine B and ferrioxamine B, (b) aHa in the keto and enol forms, and (c) possible resonance forms of aHa as a result of OH or NH deprotonation.

desB has four proton dissociation constants (pK_a) at 8.3, 9.0, 9.46, and 10.84 (measured in KCl solutions of ionic strength, 0.1 mol/dm^3), which correspond to successive deprotonation of the 3-hydroxamate groups (NOH), and the amine group (NH_3^+) (Farkas et al., 1999), respectively. The interactions of desB with Fe(III) in solution and at particle interfaces are poorly understood in the environmental pH range of 3 to 9.

A small hydroxamate siderophore analog, acetohydroxamic acid (aHa), is also used to elucidate the molecular structure of desB in aqueous solutions. Acetohydroxamic acid is an oxime that exists in either an enol or keto form and has a pK_a of 9.37 (Schwarzenbach and Schwarzenbach, 1963; Fig. 1). Theoretical studies indicate that the keto-form is dominant in aqueous solution with the *cis* conformation being more stable than the *trans* conformation (Hadzi and Prevorsek, 1957; Bagno et al., 1994). However, the deprotonation site of aHa in aqueous solutions is debated because of its two acidic protons (N-H, NO-H), and discrepancies that exist between the NMR predicted and theoretically derived structures (Fitzpatrick and Mageswaran, 1989; Ventura et al., 1993; Bagno et al., 1994; Yazal and Pang, 1999). An NMR study of aHa in aqueous solution revealed that NO-H is the primary site of deprotonation (Bagno et al., 1994), while calculations on anhydrous gas-phase aHa predicted N-deprotonation (Ventura et al., 1993; Bagno et al., 1994; Yazal and Pang, 1999). However, calculations also indicated that the addition of solvated water molecules stabilized O-deprotonated species more than the N-deprotonated species (Ventura et al., 1993). Complexation of aHa with Fe(III) shows that the $Fe(aHa)_3$ is the dominant species in the pH range of 4–10 (Holmen et al., 1997; Farkas et al., 1998), with aHa forming three five-membered rings around Fe (Monzyk and Crumbliss, 1979; Brink and Crumbliss, 1984; Crumbliss, 1990).

The goal of this research is to evaluate: 1) the stable structures of aHa and desB in aqueous solution, 2) the nature of Fe(III) complexation with aHa and desB, and 3) the influence of Fe(III) complexation on the amine and amide groups of desB that are not involved in complex formation. By combining experimental (UV-vis, IR and resonance Raman) and ab initio (DFT) analysis, the functional group chemistry of aHa and desB and the structures of their Fe(III) complexes are evaluated. This work represents part of a larger effort to characterize molecular interactions between metal ions and organic molecules in aqueous solutions and at mineral-water interfaces, and their role in various biogeochemical reactions.

2. MATERIALS AND METHODS

2.1. Preparation of Solutions

Aqueous solutions of acetohydroxamic acid (Aldrich), desferrioxamine mesylate (Sigma), $FeCl_3 \cdot 6H_2O$ (Fisher Scientific), NaOH (Fisher Scientific), and HCl (Fisher Scientific) were prepared with high purity 18 MW cm^{-1} water (Milli-Q Plus, Millipore) or 99.99% D_2O (Cambridge Isotope Lab). Aqueous solutions were prepared on a gravimetric basis, and a density of 1.00 g $\cdot$ cm^{-3} was assumed for the solution when converting to a molar scale. The concentrations of aHa and desB were kept constant at 47 ($\pm$ 2) mM, and 25 ($\pm$ 2) mM, respectively, in all the vibrational spectroscopy experiments. However, dilute solutions were used for collecting UV-vis spectra (0.4 mM aHa and 0.13 mM $FeCl_3$, and 0.045 mM desB and 0.045 mM $FeCl_3$). The pH of aHa and desB were adjusted by adding 0.01 M NaOH or HCl. Iron complexation with these ligands was examined for [aHa]/[$FeCl_3$] of 3, and [desB]/[$FeCl_3$] of 1. The pH measurements were made using an Orion 525A pH meter fitted with a semimicro pH probe. In acidic solutions, changes larger than one pH unit occurred for aHa solutions when they were stored at room temperature overnight. To minimize such pH variations, samples were stored at 4°C except when used for spectroscopic analysis. The pH (or pD) of D_2O solutions were measured with the same pH meter and then corrected it by adding 0.41 to the measured pH value (Gary et al., 1964).

2.2. UV-vis Spectroscopy

UV-vis spectra of aqueous aHa, desB, and their Fe (III) complexes were measured on a Hewlett Packard 8452A diode array spectrophotometer. The solutions were placed in quartz cuvettes and scanned in the range of 190–820 nm with water as the background. The resolution of this instrument was 2 nm.

2.3. Vibrational Spectroscopy

Aqueous solutions of aHa and desB and their Fe(III) complexes were analyzed on a Bruker IFS 66 v/s FT-IR spectrometer, using 45° ZnSe (sample pH >4.0) and AMTIR (sample pH <4.0) ATR trough plates. The setup of the spectrometer is as follows: number of reflections: 12, resolution: 2 cm^{-1}, beam entrance slit: 4 mm, scan range: 4000–700 cm^{-1}, detector: Hg-Cd-Te (MCT), number of scans: 500. A reference spectrum of deionized water was collected after each sample, and subtracted from the sample spectrum to reduce the absorption from water at 1636 cm^{-1}. For aHa and desB samples containing D_2O, a

reference spectrum of D_2O together with an aliquot of sample (without the ligands) was used as background. The spectrum of each sample is an average of five independent acquisitions (this was done to reduce the background variations caused by detector drifts). The spectral analysis was performed using the software program Grams 5.2.

Resonance Raman spectra were obtained using an excitation wavelength of 407 nm (Spectra Physics krypton laser) and a 270° backscattering sample geometry. The laser beam (power 20 mW) was focused with a cylindrical lens onto a NMR tube containing the sample, and the scattered light was collected and focused onto a single spectrograph (Chromex) equipped with a CCD (Princeton Instruments). This is an in-house built Raman spectrometer. All samples were scanned 20 times (each 30 s) and averaged. Raman bands of N,N-dimethylformamide at 1662, 1439.7, 1406.6, and 1092.4 cm^{-1} were used to calibrate all samples. The Raman spectrum of water was used to subtract water contributions from sample.

2.4. Ab Initio Calculations

The geometries of aHa and desB (only part of desB is considered because of size limitations) in different coordination environments were optimized and their vibrational frequencies were calculated at the DFT B3LYP/6-31G* level, using the Gaussian 92 package (Frisch et al., 1992). Three water molecules were placed around the deprotonation site of aHa to mimic an aqueous environment. The intensities of IR and Raman bands were evaluated from the analytical dipole moment and numerical polarizability derivatives, respectively. Calculations performed for the $Fe(aHa)_3$ complex were within C_3 symmetry constraints. A Lorentzian curve with a fixed half-width of 5 cm^{-1} was used to represent each calculated vibrational band, and its height corresponds to the calculated intensity. A single scale factor of 0.956 was applied to all calculated harmonic frequencies to account for any systematic errors due to basis set truncation or incomplete treatment of electron correlation (Baker et al., 1998). This factor was obtained from a linear least-squares fit of calculated (this study) and experimental (Lin-Vien, 1991) wave numbers for acetic acid and acetamide. These compounds were chosen based on their functional group similarities to aHa and desB.

3. RESULTS

3.1. Theoretical Studies of aHa and desB

The hydrated species considered in this investigation were: neutral *cis*-$aHa(H_2O)_3$, O-deprotonated *cis*-$aHa(H_2O)_3$, O-deprotonated *trans*-$aHa(H_2O)_3$, and N-deprotonated *cis*-$aHa(H_2O)_3$ (Fig. 2). The calculated energies of these hydrated species indicate that O-deprotonated *cis*-$aHa(H_2O)_3$ is the most stable anion (Table 1). Although the calculations of Ventura et al. (1993) predict that O-deprotonated aHa is stabilized more by the addition of water molecules when compared to the N-deprotonated aHa, their absolute energies indicate that the latter is the most stable species. The difference between the model used by Ventura et al. (1993) and this study is that they used four water molecules to mimic an aqueous environment. However, the bond distances predicted by Ventura et al. using different basis sets show the same trends with those reported here (Table 1). It is anticipated that hydrogen bonding between the NO-H and C=O in the case of N deprotonated aHa may make it more stable in the calculations conducted by Ventura et al. In the case of the $Fe(aHa)_3$ complex (Fig. 2), DFT calculations showed that the high-spin Fe(III) complex (S = 6) is energetically more favorable than the low-spin Fe(III) complex in the ground state. This is consistent with the experimental studies on the $Fe(aHa)_3$ complex (Monzyk and Crumbliss, 1979). All calculated normal modes fall into doubly degenerate ($E_{x,y}$), and total symmetric representations (A_z) within the C_3 point group. There are 30 fundamentals (10 E, 10 A) in the energy region of 900–1700 cm^{-1}). Mass exchange calculations of hydrogen with deuterium on the nitrogen atom were also computed for the selected species. The resulting calculated wavenumbers agree with the measured values (Tables 2–4).

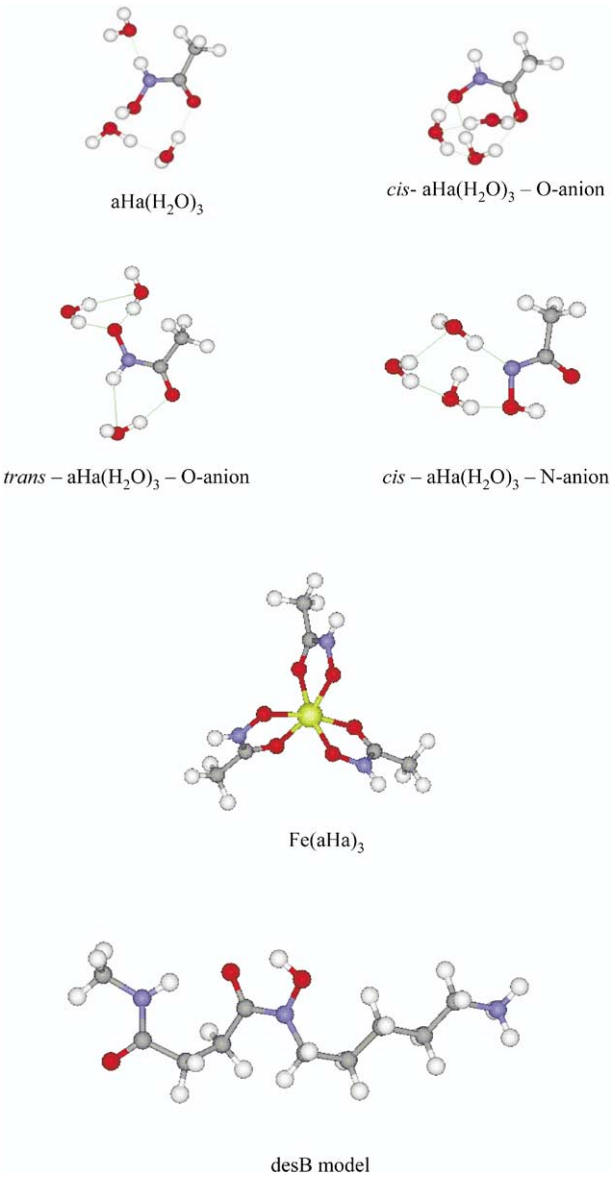

Fig. 2. Structural representations of the calculated models for aHa and desB. Color description: gray = carbon, blue = nitrogen, red = oxygen, white = hydrogen, yellow = iron. Hydrogen bonds are represented by light green lines.

Because of constraints of the number of atoms (or the size of the molecule) that can be used in Gaussian 92, calculations for desB were conducted for part of the molecule, i.e., starting at the amine group and ending with a methyl group after the first amide functional group in desB (as shown in Figs. 1 and 2). This model includes all of the major functional groups of the molecule, and the calculated vibrational frequencies (shown in Table 5) may closely represent the frequencies of the entire molecule. Since the calculations

Table 1. Calculated energies and bond lengths.

Species	Energy (kJ/mol)[a]	Bond length (Å) C=O	C-N	N-O	Fe-O (C)	Fe-O (N)
cis-aHa$(H_2O)_3$	0	1.235	1.351	1.392		
cis-aHa$(H_2O)_3$—O-anion	1438	1.258	1.336	1.351		
cis-aHa$(H_2O)_3$—N-anion	1532.9	1.267	1.329	1.455		
trans-aHa$(H_2O)_3$—O-anion	1451.4	1.266	1.332	1.368		
Fe$(aHa)_3$	—	1.264	1.326	1.356	2.108	1.966
desB model	—	1.243	1.364	1.411		

[a] The energies are all relative to *cis*-aHa$(H_2O)_3$, the most stable of the neutral species.

indicate that there are several vibrational bands from the bending vibrations of methylene groups in the fingerprint region of 900–1500 cm^{-1} (Table 5), the vibrational spectral analysis focused on the amide I band and not on the amide II, amide III or $\nu_{(N\text{-}O)}$.

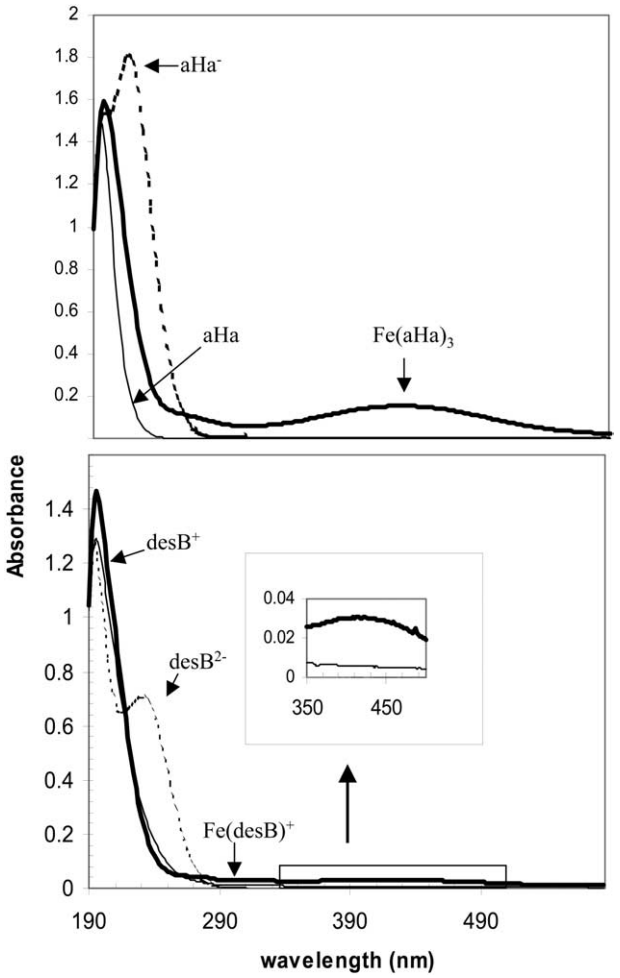

Fig. 3. UV-vis spectra for aHa (top) and desB (bottom). (top) aHa (solid line; 0.4 mM, pH = 3.68), aHa^- (dashed; 0.4 mM, pH = 10.33), and Fe$(aHa)_3$ complex (thick solid line; 0.4 mM aHa, 0.13 mM $FeCl_3$, pH = 4.0). (bottom) Neutral desB (solid line; 0.045 mM, pH = 4.07), $desB^{2-}$ (dashed; 0.045 mM, pH = 10.25), and Fe(III) complexed desB (thick solid line; 1:1 complex, pH = 4.29). Inset is enlarged view of ligand-to-metal charge transfer band of desB.

The calculated wavenumbers of the vibrational spectra are in good agreement with the experimental data. The magnitude of differences between them is the largest for amide I band of the amide group in the desB model (discrepancy of 85 cm^{-1}), and is the smallest for the $\nu_{(N\text{-}O)}$ in the Fe$(aHa)_3$ model (~6 cm^{-1}). The large difference between the experimental and the calculated wavenumbers for the amide I band may be caused by the lack of solvated water molecules around the amide and oxime groups in desB. It should also be noted that it was difficult to simulate water solvation and a hydrogen bonding environment using 3 water molecules in these calculations. This can result in the noted differences in the calculated and experimental vibrations of aHa models. However, the Fe$(aHa)_3$ calculations agree closely with the experimental vibrational band energies because all functional groups in Fe$(aHa)_3$ complex are bound to Fe(III) and H-bonding is not an issue.

3.2. Spectroscopy Studies of aHa in Aqueous Solution

3.2.1. Protonation and deprotonation of aHa

Acetohydroxamic acid absorbs at 196 nm in the neutral state (pH = 3.68), and this is attributed to the π-π^* transition of the carbonyl group (Fig. 3). This absorption band shifts to 218 nm upon aHa deprotonation. The redshift is consistent with a weakening (lengthening) of the carbonyl bond strength (Rao, 1967). The loss of a proton causes excess charge on the oxime oxygen atom, leading to conjugation in the aHa CONC core (conjugation through the carbonyl oxygen, the carbonyl carbon, and the nitrogen) to distribute this excess charge (see hydroxyl deprotonation, Fig. 1). The following vibrational spectroscopy results also corroborate these results.

The vibrational spectrum of aHa exhibits characteristic amide I ($\nu_{(C=O)}$ stretch), amide II (caused by the vibrational coupling of $\delta_{(N\text{-}H)}$bend and $\nu_{(C\text{-}N)}$ stretch (Nigtingale and Wagner, 1954), amide III (combination between $\nu_{(C\text{-}N)}$ stretching and $\delta_{(N\text{-}H)}$ rocking character), $\nu_{(N\text{-}O)}$ (oxime) stretch, and $\delta_{(CH3)}$ and $\delta_{(NOH)}$ bending modes in the wave number range of 900–1700 cm^{-1}. In this study, the amide I, $\nu_{(N\text{-}O)}$, and $\delta_{(NOH)}$ bending modes are emphasized because these moieties are directly involved in the deprotonation and Fe complexation of aHa (and in desB, discussed later). Although all other characteristic bands provide supporting evidence for the proposed structure, they will not be rigorously discussed (Tables 2–4). The $\nu_{(O\text{-}H)}$ and $\nu_{(C\text{-}H)}$ stretching vibrations overlap with the water stretching bands and are not considered in this investigation. Although the water bending mode at 1636 cm^{-1} over-

Table 2. Theoretical and experimental vibrational modes and their assignments for aHa in H_2O.[a]

Neutral aHa (cm^{-1})			aHa anion (cm^{-1})				
	Theory			Theory			
Exptl. pH = 4.89	aHa$(H_2O)_3$[b]	Assignment (%)[c]	Exptl. pH = 12.3	O-anion[d]	Assignment (%)	N-anion[e]	Assignment (%)
		amide I			amide I		
1658	1685	νC=O(41)	1612	1623	νC=O(54)	1590	νC=O(52)
	1665	νC=O(18)			νC-N(28)		νC-N(25)
		amide II			amide II		
1548	1526	δN-H rock(51)	1542	1493	νC-N (15)	1457	δCH_3 adef(52)
		δNOH bend(29)			δN-H rock (71)		δNOH bend(24)
		νC-N(5)			νC-C(4)	1444	νCH_3 adef(94)
					νC=O(5)	1430	δCH_3 adef(37)
	1506	νC-N(10)					νC-N(12)
		δN-H rock(26)					δNOH bend(44)
		δNOH bend(44)					
1448	1452	δCH_3 adef(90)	1447	1457	δCH_3 adef(90)		
1434	1439	δCH_3 adef(92)	1434	1435	δCH_3 adef(90)		
		δCH_3 rock (8)					
1377	1367	δCH_3 sdef (87)	1381	1349	δCH_3 sdef(91)	1356	νCH_3 sdef(75)
		amide III			amide III		
1318	1281	νC-N (34)	1319	1266	νC=O(17)	1307	νC=O(15)
		δN-H rock(18)			νC-N(21)		νC-N(24)
		νN-O (8)			δN-H rock (28)		δCH_3 sdef(23)
1091	1075	νN-O(59)	1096	1099	νN-O(55)	1025	δCH_3 rock(78)
		νCH_3 rock(19)			δCH_3 rock(20)	993	δCH_3 rock(67)
1043	1023	νCH_3 rock(70)	1036	1017	νCH_3 rock(73)	972	νC-C(24)
							νC=O(21)
993	969	νCH_3 rock(40)	988	946	δC-O out(10)		δCON bend(19)
		νN-O(8)			δCH_3 rock(39)		δC-O rock(12)
		νC-C(31)			δCH_3 rock(24)	894	νN-O(20)
						866	νN-O(45)

[a] sdef = symmetric deformation, adef = asymmetric deformation, rock = denotes a rocking motion, bend = bending mode, out = out of plane bend.
[b] = *cis*-aHa$(H_2O)_3$.
[c] = The compositional assignments were determined from the Gaussian calculations. The number in parentheses refers to the percent contribution each mode (stretching, bending, or rock) has on the frequency.
[d] = Oxygen deprotonated *cis*-aHa$(H_2O)_3$.
[e] = Nitrogen deprotonated *cis*-aHa$(H_2O)_3$.

laps with the amide I band, the identification of amide I band is not a problem in D_2O solutions and in the Raman spectra of aHa.

The amide I band of aHa in the neutral state (below the pKa) is at 1658 $cm^{-1}$and shifts to 1612 cm^{-1} upon deprotonation (Table 2; Figs. 4 and 5), consistent with the calculated shifts (Table 1, 2). The amide II band overlaps with the $\delta_{(NOH)}$ band and occurs at 1548 cm^{-1} for neutral aHa. Upon deprotonation, this band becomes more discrete, indicating that the $\delta_{(NOH)}$ character is lost and becomes a relatively pure amide II mode. The $\nu_{(N\text{-}O)}$ band shifts from 1091 to 1096 cm^{-1} upon aHa deprotonation, implying a shorter N-O bond length, which is also in agreement with the calculations (Table 1). Although bond length estimates indicate that the change in N-O bond length is greater than the change in the C=O bond length (Table 1), the magnitude of band shifts are small for the $\nu_{(N\text{-}O)}$ (5 cm^{-1}) when compared to that of the amide I band (~35 cm^{-1}). This small shift in $\nu_{(N\text{-}O)}$ may be caused by coupling of N-O vibrations with the methyl bending modes.

Infrared spectroscopy studies were also conducted in D_2O to complement the studies in water. The bending mode of D_2O occurs at 1200 cm^{-1} and does not interfere with the amide I band, which occurs at 1648 cm^{-1} for neutral aHa and shifts to 1618 cm^{-1} upon deprotonation. The $\nu_{(N\text{-}O)}$ stretch is coupled to $\delta_{(N\text{-}D)}$ and exhibits split peaks at 1112 and 989 cm^{-1} for neutral form, which shift to 1120 and 986 cm^{-1} upon aHa deprotonation, respectively. These bands are more discrete at higher pD, indicating stronger coupling with $\delta_{(ND)}$. Calculated vibrational bands also show similar shifts (Table 3, Figs. 4 and 5).

3.2.2. *Fe(III) complexation of aHa*

Solution speciation studies indicate that $Fe(aHa)_3$ is the dominant species in the pH range of 4–10 and for Fe(III)/aHa ratios used in this study (Holmen et al., 1997; Farkas et al., 1998). The UV-vis and vibrational spectra show interesting changes when aHa is complexed to Fe(III). While the UV-vis absorption spectrum of the $Fe(aHa)_3$ complex resembles the spectrum of neutral aHa for the p-p* transition of the carbonyl, the vibrational spectrum resembles the anionic form of aHa. The π-π* transition of the carbonyl at 198 nm in the UV-vis spectrum of neutral aHa is unchanged when aHa is complexed with Fe(III) (Fig. 3). In addition, a rela-

Table 3. Theoretical and experimental vibrational modes and their assignments for aHa in D_2O.[a]

Neutral aHa (cm^{-1})			aHa anion (cm^{-1})				
	Theory			Theory		Theory	
Exptl. pD = 5.42	aHa$(D_2O)_3$[b]	Assignment (%)[c]	Exptl. pD = 12.71	O-anion[d]	Assignment (%)	N-anion[e]	Assignment (%)
1648	1676	νC=O(77) νC-N(10)	1618	1624	νC=O(56) νC-N(29)	1584	νC=O(52) νC-N(28)
1473	1379	νC-N (38) νN-O(7) δCH_3 adef (17) δC-O rock(8) δN-D rock(12)	1375	1390	νC-N (32) νC=O(15) νC-C(12) δN-D rock (15)	1448 1445 1369	δCH_3 adef (87) δCH_3 adef (93) νC-C(18) νC=O(9) νC-N(25)
1434	1455	δCH_3 adef(76) δCH_3 rock(8)	1460	1458	δCH_3 adef(88)	 1333	δCH_3 sdef (34) δCH_3 sdef (63) νC-N(18)
1417	1439	δCH_3 adef(92)	1434	1436	δCH_3 adef(91)		νC=O(10)
1374	1363	δCH_3 sdef(88) νC-N(5)		1346	δCH_3 sdef(95)	1087	δNOD bend(77) δCON bend(18)
1112	1111	δNOD bend(64) νN-O (7)	1120	1102	νN-O(36) δCH_3 rock(25) νC-C(10)	1024 990	δCH_3 rock(79) δC-O rock (16) δCH_3 rock(71)
1091	1094	δN-D rock (28)	1094				
1041		δCH_3 rock(25) νN-O (14)	1014	1016	δCH_3 rock(73) δC-O rock(13)	873	νN-O (67)
1020	1025	δCH_3 rock (70) δC-O rock(18)	986	1000	δN-D rock(54) νN-O (30)		
989	1010	νN-O(48) δN-D rock(37)	937	941	νC-C(32) νCH_3 rock (31)		

[a] For the neutral and anionic forms of aHa, only exchange at the oxygen or nitrogen atom is assumed; the methyl group does not have exchange take place in the theoretical calculations. sdef = symmetric deformation; adef = asymmetric deformation; rock = denotes a rocking motion; bend = bending mode

[b] *cis*-aHa$(D_2O)_3$.

[c] The compositional assignments were determined from the Gaussian calculations. The number in parentheses refers to the percent contribution each mode (stretching, bending, or rock) has on the frequency.

[d] Oxygen deprotonated *cis*-aHa$(D_2O)_3$.

[e] Nitrogen deprotonated *cis*-aHa$(D_2O)_3$.

tively weak band at 430 nm corresponding to ligand-to-metal charge transfer appears in this spectrum (Farkas et al., 1998). In IR, the amide I band occurs at 1610 cm^{-1} (1613 cm^{-1} in resonance Raman) for Fe(aHa)$_3$ complex, which is similar to that of the anionic form of aHa (1612 cm^{-1}). The $\nu_{(N\text{-}O)}$ band bond in the Fe(aHa)$_3$ is also invariant upon Fe(III) complexation (1094 cm^{-1} in IR and 1097 cm^{-1} in resonance Raman; Fig. 6). The calculated bond lengths for both the C=O and N-O in Fe(aHa)$_3$ complex are similar to those in aHa^-. The amide II band at 1528 cm^{-1} is not broad, indicating that the $\delta_{(NOH)}$ mode of aHa disappears upon Fe(III) complexation. Studies in D_2O solutions also confirm the above assignments (Table 4). The vibrational spectra of Fe(aHa)$_3$ solutions were also examined at higher pH values (pH >10) to identify changes in the structure of Fe(aHa)$_3$ complex. The noticeable difference between the low and high pH samples was the increase in the number of Raman active peaks in the latter. This may suggest a change in the coordination, structure, or symmetry of the Fe(aHa)$_3$, which should result in the appearance of more fundamental vibrational bands in the spectra. In addition, a new band at 1560 cm^{-1} appears in both H_2O and D_2O solutions, and this may be due to N-deprotonation (data not shown) or to the formation of an Fe(III)-hydroxamido complex.

3.3. Spectroscopy Studies of desB in Aqueous Solution

3.3.1. Protonation and Deprotonation of desB

The spectral variations of desB are similar to those reported for aHa. The π-π* transition of the carbonyl in desB is at 196 nm in acid solutions and shifts to 230 nm as the solution pH is increased. The greater redshift (by ~10 nm more) in desB, when compared to aHa, may be caused by more conjugation in the carbonyl oxygen that stabilizes the negative charge on the oxime group (conjugation through the carbonyl oxygen, the carbonyl carbon and the nitrogen). In addition, the electron donating ability of the long chain carbon group attached to the nitrogen atom in desB, when compared to the hydrogen atom in aHa, promotes enhanced conjugation in CONO core of desB. The π-π* transition of the amide group also occurs at 194 nm, and becomes more evident when the oxime groups are fully deprotonated in alkaline solutions. In the vibrational spectra, aqueous desB exhibits two different $\nu_{(C=O)}$ modes: i) oxime related amide I band at 1605 cm^{-1} in neutral desB, which shifts to 1579 cm^{-1} in the anionic form (Figs. 7 and 8, Table 5), and ii) amide related band around 1620 cm^{-1}, which is not affected by deprotonation significantly. Overlap of the $\nu_{(C=O)}$ stretch of the amide and oxime groups complicates the identification of

Table 4. Experimental and theoretical vibrational modes for the Fe(aHa) complex in H_2O and D_2O.[a]

Experimental frequencies (cm^{-1})				Calculated frequencies (cm^{-1})				
IR		Raman		Sym[c]: Calc.[d]		Intensity[b]		
H_2O	D_2O	H_2O	D_2O	N-H	N-D	IR	Raman	Assignment
								amide I
1610	1594	1613	1594	A: 1583	1580	177.6	208.5	νC=O stretch
				E: 1572	1568	102.4	118.3	νC-N stretch
								amide II
1528	1474	1531	1475	A: 1509	1471	23.1	98.8	δN-H rock
				E: 1507	1469	25.2	38.3	νC=O stretch
								νC-N stretch
1440	1434	1438	1437	A: 1446	1432	54.6	21.4	δCH_3 adef
				E: 1446	1433	23.2	17.3	
1440	1434	1438	1437	A: 1431	1431	5.5	0.1	δCH_3 adef
				E: 1431	1431	7.5	27.3	
1389	1398	1388	N/A	A: 1375	1371	4.1	16.7	δCH_3 sdef
				E: 1375	1369	3.1	20.2	
								amide III
1336	952	1333	N/A	A: 1271	908	5.2	16.9	δN-H rock
				E: 1268	908	28.8	4.7	
1094	1133	1097	1135	A: 1100	1119	109.7	63.9	νN-O
				E: 1098	1116	54.7	27.9	
1039	1042	N/A	1026	A: 1024	1024	2.4	0.05	δCH_3 rock
				E: 1025	1025	6.6	0.1	
999	994	995	994	A: 980	981	50.8	15.1	δCH_3 rock
				E: 979	979	9.7	5.1	νC-C
								νC-N
								νN-O
983	971	N/A	N/A	A: 958	978	1.2	1.6	δCH_3 rock
				E: 958	977	1.5	7.6	5- membered ring bend

[a] sdef = symmetric deformation; adef = asymmetric deformation; rock = rocking motion.
[b] Intensity of the peak in off-resonance Raman and IR.
[c] Symmetry of the frequency in the $Fe(aHa)_3$ model.
[d] Calculated frequency of the symmetry mode.

the $\nu_{(C=O)}$ of amide group of neutral desB in aqueous solutions (Fig. 7). However, the anionic form of desB exhibits two distinct peaks at 1622 cm^{-1} and 1582 cm^{-1} in D_2O solutions, which are assigned to the amide and oxime $\nu_{(C=O)}$ stretching modes, respectively. The infrared spectra calculated using the desB model verifies that the amide carbonyl is at a higher wave number than the oxime carbonyl in the neutral form (Fig. 7).

3.3.2. *Fe(III) Complexation of desB*

Like the Fe-aHa complex discussed above, the UV-vis absorption spectrum of carbonyls (π-π* transitions) in Fe-desB complex is similar to that of neutral desB (Fig. 3), and the vibrational band of the oxime carbonyls of Fe-desB is similar to that of the anionic form of desB (Fig. 8). The charge-transfer band of Fe-(desB) complex occurs at 420 nm, which is blueshifted by 10 nm when compared to that of the $Fe(aHa)_3$ complex. This suggests that the ligand field stabilization is greater in Fe-desB than the $Fe(aHa)_3$ complex. In the infrared spectrum, the $\nu_{(C=O)}$ stretch of the Fe(III)-desB complex exhibits two bands at 1627 cm^{-1} and 1577 cm^{-1}, which correspond to the amide and oxime carbonyls, respectively (Fig. 8), and these are similar to those reported for the anionic desB. resonance Raman (sensitive to the moieties bonded to the Fe(III)) spectrum of Fe-desB show distinct bands at 1579 cm^{-1} and 1209 cm^{-1}, which are identified unambiguously as the oxime carbonyl, and the $\nu_{(N\text{-}O)}$ stretch, respectively (Fig. 8). The $\nu_{(N\text{-}O)}$ stretch is blueshifted by 118 cm^{-1} in desB when compared to aHa, and this is a direct result of substitution effects on the oxime nitrogen.

4. DISCUSSION

Ab initio calculations and electronic and vibrational spectroscopy results were useful in the identification of the most likely conformations of aHa, and variations in the functional group chemistry of aHa and desB as a function of pH. This spectral information was used in interpreting Fe(III) complexation by aHa and desB. Since the spectral variations are similar for aHa and desB, they are discussed together in the following section.

4.1. Speciation of aHa and its Fe(III) Complexes in Aqueous Solutions

The dominant form of the neutral keto aHa in aqueous solution is identified as *cis*-aHa, since the calculated energy for the *cis* form is ~3.5 kJ/mol less than the *trans*-aHa form. The ab initio vibrational spectrum of *trans*-aHa (data not shown) indicates that the amide II and III bands (strong contributions

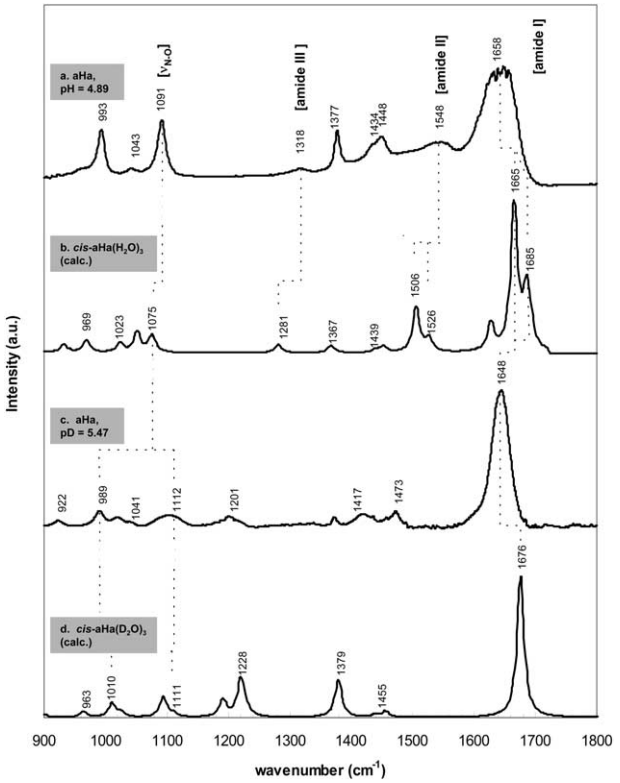

Fig. 4. ATR-FTIR spectra of neutral aHa (50 mM) in H_2O and D_2O. (a) pH = 4.89 (experimental), (b) *cis*-aHa$(H_2O)_3$ (calculated), (c) aHa in D_2O at pD = 5.47 (experimental), (d) *cis*-aHa$(D_2O)_3$ (calculated).

from N-H vibrations) shift to lower energies than those of the *cis* form because there is stronger H-bonding between N-H and C=O in *trans*-aHa. Absence of such strong redshifts in the experimental spectrum of aHa (Figs. 4a and 5a) rules out the presence of detectable *trans*-aHa and suggests that the *cis*-aHa is the dominant species in aqueous solutions at pH values below the pK_a.

As aHa deprotonates in aqueous solutions, the $\nu_{(C=O)}$ stretch and the π-π^* transition of the carbonyl are redshifted, indicating that the C=O is weakening and the C-O bond distance increases. Deprotonation at the OH or NH sites can cause these variations in C=O. The question is, where does deprotonation occur, at the N? or at the oxime O?

The $\nu_{(N-O)}$ stretch, together with the ab initio analysis, provide clues to the site of deprotonation. However, it is important to correctly identify the location of the $\nu_{(N-O)}$ band in aHa. In this study, the $\nu_{(N-O)}$ stretch is assigned to a band at 1091 cm^{-1} for aqueous aHa based on the calculations, IR and resonance Raman analysis. This contradicts the previous report of Holmen et al. (1997), who assigned the $\nu_{(N-O)}$ stretch to a band at 994 cm^{-1}. All calculations of aHa models in our study indicate that the $\nu_{(N-O)}$ stretch is strongly coupled to the $\delta_{(CH3)}$ bending and rocking vibrations and occurs in the range of 1075–1097 cm^{-1}. Only N-deprotonated aHa exhibits this band at 866 cm^{-1} (Tables 2, 3). The unequivocal experimental evidence for this assignment comes from the resonance Raman spectra of the Fe-aHa complexes. Because of the direct involvement of the NO group in the Fe(III) complex, the $\nu_{(N-O)}$ stretch is enhanced in the resonance Raman spectra and appears as a strong peak at 1097 cm^{-1}. The $\nu_{(N-O)}$ stretch of aHa also strongly couples with the $\delta_{(N-D)}$ bending mode in D_2O solutions, and results in the splitting of the $\nu_{(N-O)}$ stretch. Both ab initio and experimental studies show the splitting of the oxime band in neutral aHa and anionic aHa, supporting the above observations (Figs. 4 and 5; Table 3). The $\nu_{(N-O)}$ stretch of aqueous aHa shifts to higher energy with deprotonation. Theoretical calculations indicate that N-deprotonation should result in the lengthening of the N-O bond length, while O-deprotonation shows a decrease in the N-O bond length (Table 1), further confirming O-deprotonation of aHa in aqueous solutions.

The structure of O-deprotonated aHa can be identified using the vibrational band position of the amide II band. According to the calculated spectra, the H atom on the N atom interacts with the carbonyl oxygen in the *trans* configuration (partial intramolecular hydrogen bonding), and leads to a weaker coupling between the C-N and N-H bonds when compared to the *cis* configuration of aHa^-. Since the experimental spectra of aHa solutions do not indicate that this is occurring, the O-deprotonated form of *cis*-aHa^- is considered as the dominant conformation in aqueous solution.

Infrared and resonance Raman spectra of Fe-aHa solutions suggest that the spectra of aHa^- and $Fe(aHa)_3$ are similar, which indicate that the electronic structural changes in the

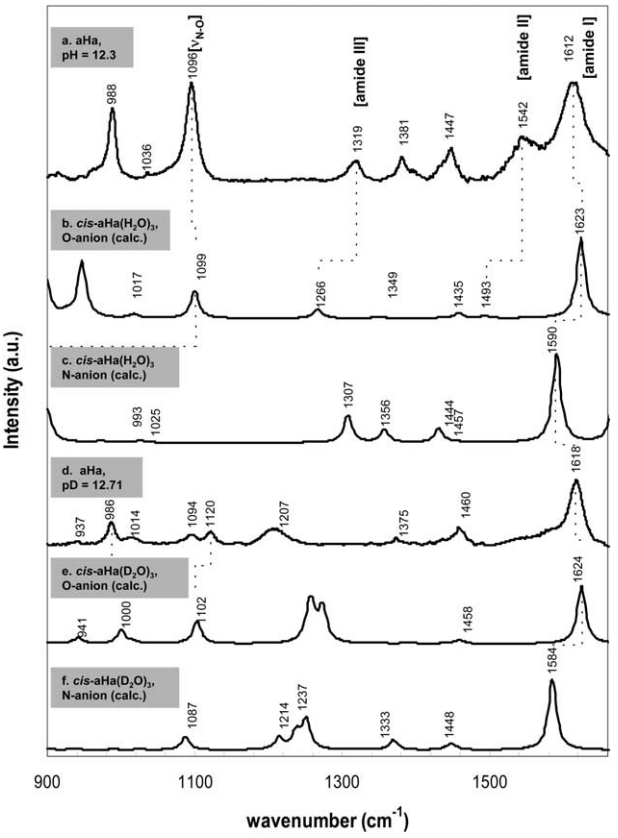

Fig. 5. ATR-FTIR spectra of anionic aHa (50 mM) in H_2O and D_2O. (a) pH = 12.3 (exp.), (b) O-deprotonated *cis*-aHa$(H_2O)_3$ (calc.), (c) N-deprotonated *cis*-aHa$(H_2O)_3$ (calc.), (d) aHa in D_2O at pD = 12.71 (exp.), (e) O-deprotonated *cis*-aHa$(D_2O)_3$ (calc.), and (f) N-deprotonated *cis*-aHa$(D_2O)_3$ (calc.).

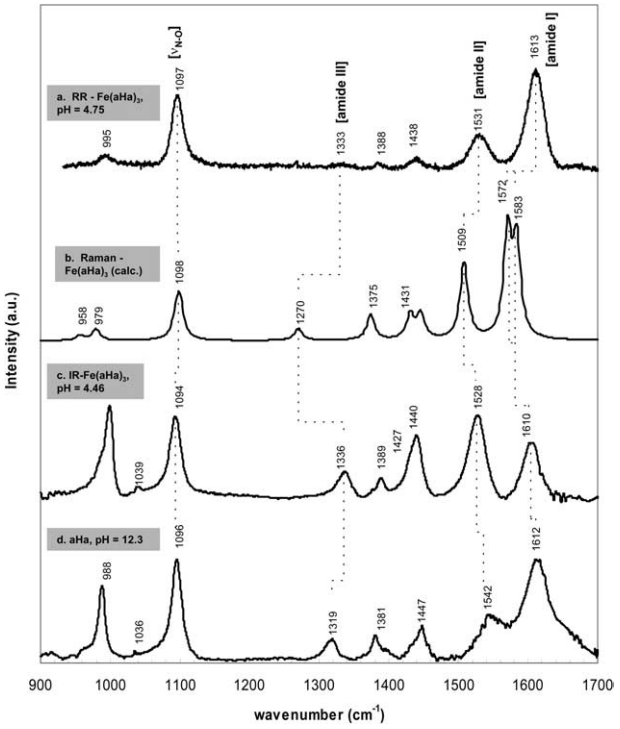

Fig. 6. Resonance Raman (a, b) and ATR-FTIR (c, d) spectra of Fe-aHa complexes in water (excitation = 407 nm for resonance Raman experiments). (a) aHa:$FeCl_3$ ratio = 3:1, pH = 4.75, 50 mM aHa (exp.); (b) Raman spectrum of $Fe(aHa)_3$ model (calc.); (c) aHa:$FeCl_3$ ratio = 3:1, pH = 4.46, 50 mM aHa (exp.); (d) aHa^- in water (pH = 12.3, 50 mM aHa, exp.). The x-axis shows energy in the form of wave number (or Raman shift in the case of resonance Raman).

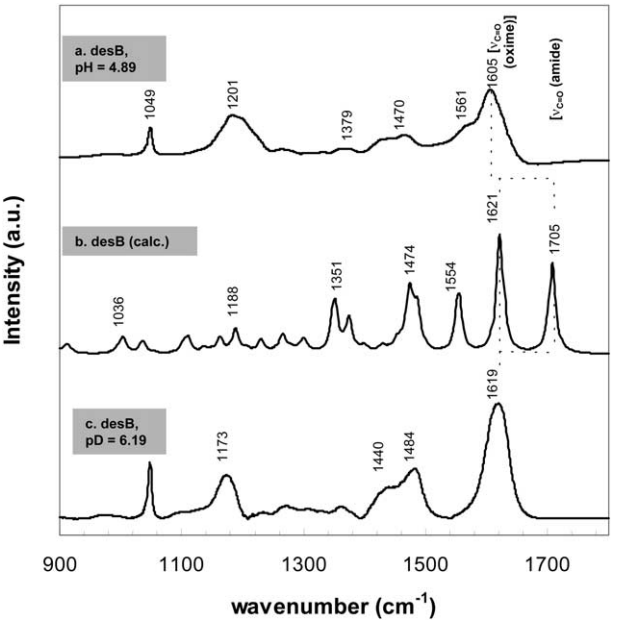

Fig. 7. ATR-FTIR spectra of desB in H_2O and D_2O. (a) 50 mM desB in H_2O at pH = 4.89 (exp.), (b) desB model (calc.), (c) 50 mM desB in D_2O at pD = 6.19 (exp.).

oxime and carbonyl groups of anionic aHa are small upon Fe(III) complexation. These spectral changes are also in agreement with the ab initio calculations. However, the π-π^* transition (from the UV-vis spectra) of the carbonyl in aHa^- shifted to high energy upon Fe(III) complexation, and this energy is similar to that of neutral aHa. This discrepancy in the vibrational and electronic spectra may be caused by the contributions from the C-N bond and π-back-bonding within the Fe-complex.

4.2. Speciation of desB and Its Fe(III) Complexes in Aqueous Solutions

The strong coupling of the methylene groups in desB when compared to aHa made it difficult to assess all of the vibrational bands in desB. Hence, this discussion focuses on the carbonyls in desB (the amide and oxime carbonyls). The infrared spectra of aqueous desB show that the vibrational bands of the amide and oxime carbonyls overlap significantly, although the ab initio calculations indicate that the $\nu_{(C=O)}$ stretch of the amide carbonyl is at a higher wave number than the oxime carbonyl (Figs. 7 and 8; Table 5). Poor separation of these bands in aqueous solutions may be caused by the problems associated with background subtraction for water in the H_2O bending region. Water normalization is not an issue in alkaline D_2O solutions, where these carbonyl bands are well separated (Fig. 8).

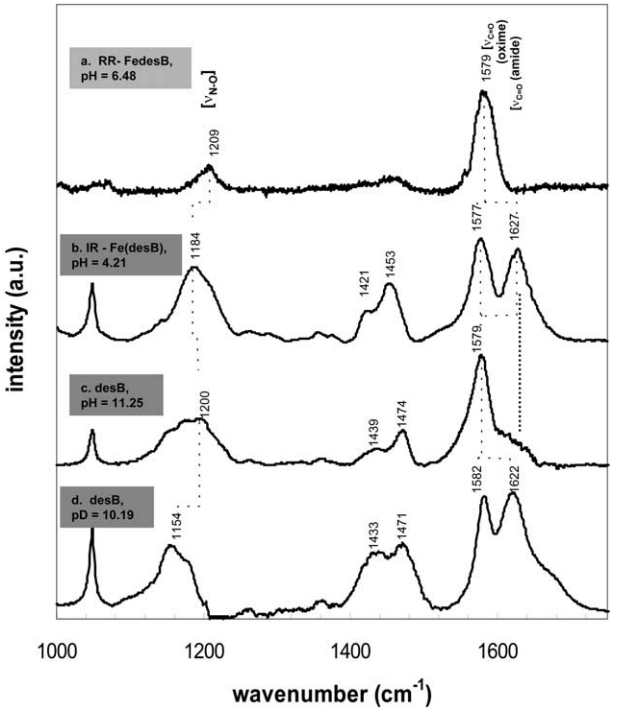

Fig. 8. Experimental resonance Raman (a) and ATR-FTIR spectra (b–d) of aqueous Fe(III)-desB complexes in H_2O and D_2O. (a) desB:$FeCl_3$ ratio = 1:1, pH = 6.48; (b) desB:$FeCl_3$ ratio = 1:1, pH = 4.21; (c) 50 mM desB at pH = 11.25; and (d) 50 mM desB in D_2O at pD = 10.19. The x-axis shows energy in the form of wave number (or Raman shift in the case of resonance Raman).

Table 5. Theoretical and experimental vibrational modes for DesB in water and when complexed with iron.[a]

Neutral DesB (cm^{-1})			Anion	Fe complex
	Theory			
Exptl. pH = 4.89	desB model[b]	Assignment (%)[c]	Exptl. pH = 11.25	Exptl. 1-1 desB:$FeCl_3$ pH = 4.21
	1705	νC=O (amide)(79) νC-N (amide)(8)	~1620 (shoulder)	1627
1605	1621	νC=O (oxime)(76)	1579	1577
1561	1554	δN-H rock (amide)(63) νC-N(amide)(15) δCH_3 rock (8)		
1470	1486	δNOH bend (oxime)(55) νC-N (oxime)(19) νC-N (adjacent to oxime)(14)	1474	1453
1444	1474	δN-H sdef (teminal N)(80) δC-H scissors(13)		
1426	1427	δCCN bend (80) δCCC bend (15)	1439	1421
	1399	δCH_3 sdef (88)		
1379	1375	νC-N (oxime)(18) δC-H wag (17) δN-H rock (terminal N)(16) δC-H twist (8)	1375	1374
1358	1351	δC-H wag (58) δC-H twist (8)	1361	1355
1201			1200	1209
1181	1188	δC-H twist (54) δC-H wag (12)	N/A	1184
1049	1036	νC-C (29) νC-N (8)	1049	1049

[a] Vibrations with less than 5% contribution to the frequency are not included. sdef = symmetric deformation; scissors = scissor bending mode; bend = bending mode; wag = methylene bending mode; twist = methylene twisting mode; rock = rocking bending mode.
[b] desB model.
[c] Number in parentheses refers to the percent contribution each mode (stretching, bending, or rock) has on the frequency.

The $\nu_{(C=O)}$ stretch of the oxime group is 50 cm^{-1} lower than the $\nu_{(C=O)}$ band in aHa, and this is attributed to the differences in the structure of the hydroxamate group in aHa and desB. According to the calculated bond distances in the desB model, the C=O (and N-O) bonds are longer in desB (Table 1). The longer bond lengths correspond to lower wavenumbers in the IR spectra and this factor may be attributed to the differences in the substituents on the nitrogen atom. With an increase in pH, the oxime carbonyl shifts to lower wavenumber because of the weakening of the C=O character. The redshifts in the UV-vis absorption spectrum of desB also suggests the same.

Complexation of desB with Fe(III) results in: i) a shift of ~30 cm^{-1} in the $\nu_{(C=O)}$ stretch of oxime carbonyl when compared to the neutral desB, ii) a rather noticeable change in the $\nu_{(C=O)}$ stretch of the amide carbonyl, and iii) a distinct $\nu_{(N-O)}$ stretch in resonance Raman at 1209 cm^{-1} (Fig. 8). These spectral variations give insight into the variations in the strengths of the $Fe(aHa)_3$ and Fe-desB complexes. The amide I band of Fe-desB complex is at 1577 cm^{-1} in Fe-desB, which is similar to the deprotonated desB (1579 cm^{-1}, Fig. 8). Because the amide I band of Fe-desB is at a much lower energy than that of $Fe(aHa)_3$ (Fig. 6), it can be inferred that the conjugation in the CONO core is greater in desB than in aHa. The large change in the $\nu_{(N-O)}$ band can also be attributed to the increased conjugation as well as the substituent attached to the nitrogen atom. When compared to the $\nu_{(N-O)}$ band of these compounds (aHa and desB), N-methyl aHa shows this band at 1167 cm^{-1} (Brown et al., 1979). In aHa, there is a hydrogen atom attached to the N, while in N-methyl acetohydroxamic acid and desB a methyl group and a long hydrocarbon chain are attached, respectively. The carbon groups in the latter two compounds are electron donating, adding more electron density to the complexation site. This adds more conjugation in the CONO core of desB than in aHa, and accounts for the decrease in energy for the amide I and increase in the energy of the $\nu_{(N-O)}$ modes. This substitution also influences their binding constants. The complexation constants (log K, where K = stability constant) of Fe(III) with aHa, N-methyl aHa and desB are 28.8, 29.4, and 32.6, respectively (Schwarzenbach and Schwarzenbach, 1963; Farkas et al., 1998). The spectral variations and differences in conjugation within the oxime group of these compounds explain these observed differences in complexation.

5. SUMMARY AND CONCLUSIONS

The functional group chemistry of aHa and desB, and their Fe(III) complexes were characterized using vibrational (infrared and resonance Raman) and electron (UV-vis) spectroscopy methods. The proposed structures and the deprotonation sites in aHa, and metal bonding environments of aHa and desB were also corroborated with the ab initio calculations. The summary of our observations is as follows,

1) The most stable form of aHa in aqueous solution is the *cis*-keto configuration, and deprotonation occurs at the O-

site. However, deprotonation may occur at the N-site in highly alkaline solutions of pH >11.0. A combination of infrared and Resonance Raman spectra, and ab initio calculations were helpful in making band assignments unambiguously and in arriving at these conclusions.

2) Changes associated with the deprotonation of oxime group are similar for aHa and desB. However, the vibrational and electronic spectra indicate that electron delocalization is stronger in desB, and this may be caused by the differences in substitution at the N-site (i.e., a proton in aHa, and long aliphatic chain in desB).
3) Differences in electron delocalization in the CONO core of the reactive oxime group in aHa and desB may lead to the significant differences in their binding constants. Stronger electron delocalization and increased conjugation in the CONO core of desB is responsible for very high Fe(III) binding constants.

The molecular information presented here is important in assessing the metal binding affinities of different hydroxamate siderophores and the chemical states of their metal complexes. This information is also useful in synthesizing different siderophore analogues, which have high affinity for specific metals, such as actinides, and in selective sequestration of these metals from waste repositories. Recently, researchers have focused on the specific interactions of siderophores with different mineral substrates (Kraemer et al., 1999). Although siderophores have high affinity for Fe(III) in aqueous solutions, these studies indicate that siderophores alone do not increase the dissolution kinetics of Fe(III)-hydr(oxides) because of steric limitations of large ligands at mineral-water interfaces,. Information presented here for solution complexes of Fe(III) is useful in interpreting the nature of siderophore interactions on Fe(III)-hydr(oxide) surfaces.

Acknowledgments—The research was funded by the EMSP program of the DOE. SBN gratefully acknowledges a postdoctoral fellowship from the Danish Natural Science Research Council (grant no. 21-0101242). The authors would like to thank Drs. J. Majzlan and S.J. Traina for reviewing the manuscript and providing critical comments.

Associate editor: W. Casey

REFERENCES

Bagno A., Comuzzi C., and Scorrano G. (1994) The Site of Ionization of Hydroxamic Acid Probed by Heteronuclear NMR Relaxation Rate and NOE Measurements. An experimental and theoretical study. *J. Am. Chem. Soc.* **116,** 916–924.

Baker J., Jarzecki A. A., and Pulay P. (1998) Direct Scaling of Primitive Valence Force Constants: An Alternative Approach to Scaled Quantum Mechanical Force Fields. *J. Phys Chem. A* **102,** 1412–1424.

Barbeau K., Rue E.L., Bruland K.W., Butler A. (2001) Photochemical cycling of iron in the surface ocean mediated by microbial iron (III) binding ligands. *Nature* **413,** 409–413.

Bergeron R. F. and Pegram J. J. (1988) An Efficient Total Synthesis of Desferrioxamine B. *J. Org. Chem.* **53** (*14*), 3131–3134.

Bergeron R. F. and Brittenham G. M. (1994) The Development of Iron Chelators for Clinical Use. CRC Press.

Boily J.F., Persson P., Sjöberg S. (2000) Benzenecarboxylate surface complexation at the goethite (α-FeOOH)/water interface: II. Linking IR spectroscopic observations to mechanistic surface complexation models for phthalate, trimellitate, and pyromellitate. *Geochim Cosmochim Acta* **64** (*20*), 3453–3470.

Bossier P., Hofte M., and Verstraete W. (1988) Ecological Significance of Siderophores in Soil. *Adv. Microbial Ecol.* **10,** 385–414.

Brainard J. R., Strietelmeier B. A., Smith P. H., Langston-Unkefer P. J., Barr M. E., and Ryan R. R. (1992) Actinide Binding and Solubilization of Microbial Siderophores. *Radiachim. Acta* 58/59, 357–363.

Brink C. P. and Crumbliss A. L. (1984) Kinetics, Mechanism, and Thermodynamics of Aqueous Iron (III) Chelation and Dissociation: Influence of Carbon and Nitrogen Substituents in Hydroxamic acid Ligands. *Inorg. Chem.* **23,** 4708–4718.

Brown D. A., McKeith D., Glass W. K. (1979) The infrared spectra of monohydroxamic acid complexes of copper, iron and nickel. *Inorg. Chim. Acta* **35,** 57–60.

Crumbliss A. L. (1990) Iron bioavailability and the coordination chemistry of hydroxamic acids. *Coord. Chem. Rev.* **105,** 155–179.

Dhungana S., White P. S., and Crumbliss A. L. (2001) Crystal Structure of ferrioxamine B: a comparitive analysis and implications for molecular recognition. *J. Biol. Inorg. Chem.* **6,** 810–818.

Duckworth O.W., Martin S.T. (2001) Surface complexation and dissolution of hematite by C1-C6 dicarboxylic acids at pH = 5.0. *Geochim. Cosmochim. Acta* **65** (*23*), 4289–4301.

Farkas E., Enyedy E. A., and Csoka H. (1999) A comparison between the chelating properties of some dihydroxamic acid, desferrioxamine B and acetohydroxamic acid. *Polyhedron* **18,** 2391–2398.

Farkas E., Kozma E., Petho M., Herlihy K. M., and Micera G. (1998) Equilibrium Studies on Copper(II)- and iron(III)- monohydroxamates. *Polyhedron* **17** (*19*), 3331–3342.

Fitzpatrick N. J. and Mageswaran R. (1989) Theoretical Study of Hydroxamic Acids. *Polyhedron* **8** (*18*), 2255–2263.

Frisch M. J., Trucks G. W., Head-Gordon M., Gill P. M. W., Wong M. W., Foresman J. B., Johnson B. C., Schlegel H. B., Robb M. A., Replogle E. S., Gomperts R., Andres J. L., Raghavachari K., Binkley J. S., Gonzalez C., Martin R. L., Fox D. J., Defrees D. J., Baker J., Stewart J. J. P., and Pople J. A. (1992) Gaussian 92, Revision C. Gaussian Inc.

Gary R., Bates R. G., and Robinson R. A. (1964) Second Dissociation Constant of Deuteriophosphoric Acid in Deuterium Oxide from 5 to 50 degrees Celsius. Standardization of a pD scale. *J. Phys. Chem.* **68** (*12*), 3806–3809.

Hadzi D. and Prevorsek D. (1957) Infra-red absorption bands associated with the NH group-III: Hydroxamic acids and derivatives. *Spectrochim. Acta* **10,** 38–51.

Hersman L., Lloyd T., and Sposito G. (1995) Siderophore-promoted dissolution of hematite. *Geochim. Cosmochim. Acta* **59** (*16*), 3327–3330.

Holmen B. A., Tejedor-Tejedor M. I., and Casey W. M. (1997) Hydroxamate Complexes in Solution and at the Goethite-Water Interface: A Cylindrical Internal Reflection Fourier Transform Infrared Spectroscopy Study. *Langmuir* **13,** 2197–2206.

Hossain M. B., Jalal M. A. F., vanderHelm D., Shimizu K., and Akiyama M. (1998) Crystal structure of retro-isomer of the siderophore Desferrioxamine E. *J. Chem. Cryst.* **28** (*1*), 53–56.

Hossain M. B., vanderHelm D., and Poling M. (1983) The Structure of Desferrioxamine E (Nocardamin), * a Cyclic Trihydroxamate. *Acta Cryst.* B39, 258–263.

Kalinowski B. E., Liermann L. J., Givens S., and Brantley S. L. (2000) Rate of bacteria-promoted solubilization of Fe from minerals: a review of problems and approaches. *Chem. Geol.* **169,** 357–370.

Kraemer S. M., Cheah S. F., Zapf R., Xu J., Raymond K. N., and Sposito G. (1999) Effect of hydroxamate siderophores on Fe release and Pb(II) adsorption by goethite. *Geochim. Cosmochim. Acta* **63** (*19/20*), 3003–3008.

Lin-Vien D. (1991) The Handbook of Infrared and Raman Characteristic Frequencies of Organic Molecules. Academic Press.

Loring J.S., Karlsson M., Fawcett W.R., Casey W.H. (2000) Attenuated total reflection–Fourier-transform infrared and ^{27}Al–nuclear magnetic resonance investigation of speciation and complexation in aqueous Al(III)–picolinate solutions. *Geochim. Cosmochim Acta* **64** (*24*), 4115–4129.

Matzanke B. F., Muller-Matzanke G., and Raymond K. N. (1989) Siderophore Mediated Iron Transport. In Iron Carriers and Iron Proteins (ed. T. M. Loehr), pp. 124. VCH.

Monzyk B. and Crumbliss A. L. (1979) Mechanism of Ligand Substitution on High-Spin Iron (III) by Hydroxamic Acid Chelators. Thermodynamic and Kinetic Studies on the Formation and Dissociation of a Series of Monohydroxamatoiron (III) Complexes. *J. Am. Chem. Soc.* **101** (*21*), 6203–6213.

Neilands J. B. (1981) Microbial Iron Compounds. *Ann. Rev. Biochem.* **50,** 715–731.

Nightingale R. E. and Wagner E. L. (1954) The Vibrational Spectra and Structure of Solid Hydroxylamine and Deutero-Hysroxylamine. *J. Chem. Phys.* **22** (*2*), 203–208.

Powell P. E., Cline G. R., Reid C. P. P., and Szaniszlo P. J. (1980) Occurrence of hydroxamate siderophore iron chelators in soils. *Nature* **287,** 833–834.

Rao C. N. R. (1967) Ultra-Violet and Visible Spectroscopy. Butterworths & Co., Ltd.

Santos M. A., Esteves M. A., Candida M., Vaz T., and Gonzalves M. L. S. S. (1993) Siderophore Analogues. Chelating properties of a new cyclic diazadihydroxamic acid. *Inorg. Chim. Acta* **214,** 47–55.

Schwarzenbach G. and Schwarzenbach K. (1963) Hydroxamatkomplexe I. Die Stabilitat der Eisen(III)-Komplexe einfacher Hydroxamsauren und des Ferrioxamins B. *Helv. Chim. Acta* **46,** 1390–1400.

Strathmann T.S., Myneni S.C.B. (2004) Speciation of aqueous Ni(II)-carboxylate and Ni(II)-fulvic acid solutions: Combined ATR-FTIR and XAFS analysis. *Geochim. Cosmochim. Acta* **68** (*17*), 3441–3458.

Stumm W. and Sulzberger B (1992). The cycling of iron in natural environments: Considerations based on laboratory studies of heterogeneous redox processes. *Geochim. Cosmochim. Acta* **56,** 3233–3257.

vanderHelm D. and Poling M. (1976) The Crystal Structure of Ferrioxamine E. *J. Am. Chem. Soc.* **98** (*1*), 82–86.

Ventura O. N., Rama J. B., Turi L., and Dannenberg J. J. (1993) Acidity of Hydroxamic Acids: An ab initio and Semiempirical Study. *J. Am. Chem. Soc.* **115,** 5754–5761.

Yazal J.E. and Pang Y.-P. (1999) Novel Stable Configurations and Tautomers of the Neutral and Deprotonated Hydroxamic Acids Predicted from High-Level ab Initio Calculations. *J. Phys. Chem. A* **103,** 8346–8350.